



Swansea University
Prifysgol Abertawe



Cronfa - Swansea University Open Access Repository

This is an author produced version of a paper published in :

Corrosion

Cronfa URL for this paper:

<http://cronfa.swan.ac.uk/Record/cronfa31999>

Paper:

Williams, G., Ap Llwyd Dafydd, H., Subramanian, R. & McMurray, N. (2017). The influence of Chloride Ion Concentration on Passivity Breakdown in Magnesium. *Corrosion*

<http://dx.doi.org/10.5006/2328>

This article is brought to you by Swansea University. Any person downloading material is agreeing to abide by the terms of the repository licence. Authors are personally responsible for adhering to publisher restrictions or conditions. When uploading content they are required to comply with their publisher agreement and the SHERPA RoMEO database to judge whether or not it is copyright safe to add this version of the paper to this repository.

<http://www.swansea.ac.uk/iss/researchsupport/cronfa-support/>

The influence of Chloride Ion Concentration on Passivity Breakdown in Magnesium

G. Williams*, H. Ap Llwyd Dafydd, R. Subramanian and H.N. McMurray

*Materials Research Centre, College of Engineering, Swansea University, Bay Campus,
Crymlyn Burrows, Swansea SA1 8EN, United Kingdom*

Abstract: An empirically derived dependence of an apparent breakdown potential (E_b) of magnesium (Mg) on chloride ion concentration is reported. In situations where spontaneous breakdown in the absence of external polarization is observed, leading to the subsequent propagation of localised corrosion, E_b can be determined by following time-dependent changes in free corrosion potential (E_{corr}). Breakdown of temporary passivity is marked by a clear inflection in the time-dependent value of E_{corr} , characterised by a sharp decrease in potential from a maximum value where $E_{\text{corr}} = E_b$. Characterisation of localized corrosion behaviour by in-situ scanning vibrating electrode studies, prior to and following the point of breakdown, is employed to explain the observed E_{corr} vs. time characteristics. Examples of typical behaviour upon immersion in aqueous solutions containing different chloride ion concentrations ($[\text{Cl}^-]$) are given for commercially pure Mg and an AZ31 alloy. For high purity Mg, which remains passive at pH 11 at all chloride concentrations $\leq 2 \text{ mol dm}^{-3}$, E_b values are determined as a function of chloride ion concentration $[\text{Cl}^-]$ by means of a potentiodynamic method. In both cases a dependence of E_b on $[\text{Cl}^-]$ is established such that $E_b = A + B \log_{10}[\text{Cl}^-]$, where the value of B is typically -0.11 V per decade. The practical implications of the existence of a breakdown potential for Mg is considered in terms of the selection of an appropriate chloride ion concentration in standard corrosion tests.

* Corresponding author: geraint.williams@swansea.ac.uk, Tel: +44 (0)1792 295589

1. Introduction

Although magnesium (Mg) is the fourth most abundant element on earth, its widespread use as a structural metal has yet to be realized because of its poor corrosion resistance¹⁻⁸. Only through a comprehensive understanding of the various phenomena which comprise the magnesium corrosion mechanism will routine usage of next-generation, intrinsically corrosion resistant Mg based alloys become reality. Magnesium is not typically considered to exhibit passive behavior and passivity breakdown in a manner similar to metals such as stainless steel and aluminum, leading to subsequent highly localized forms of corrosion such as pitting⁹. However, recent studies using in-situ scanning vibrating electrode technique (SVET) measurements on Mg and its alloys, immersed in chloride containing electrolytes under freely corroding conditions, have revealed temporary passive behavior prior to an apparent breakdown in passivity¹⁰⁻¹⁴. This is shown to involve the appearance of a dark spot on the exposed surface, coinciding with the location of highly focal region of intense net anodic activity¹⁰. As such, the process of apparent breakdown resembles that of other passive metals such as aluminum and stainless steel, although the subsequent propagation of localized corrosion is shown to diverge significantly for Mg, producing local anodes which move away from their original point of initiation¹⁰⁻¹⁴.

For metals and alloys which are susceptible to passivity breakdown, resistance to corrosion is typically characterized by the pitting or breakdown potential (E_b), which represents the potential above which stable pitting will occur under well-defined conditions of temperature, pH and aggressive ion (e.g. chloride) concentration¹⁵. Many publications have demonstrated that E_b becomes progressively more negative with increasing chloride ion concentration ($[Cl^-]$) for a range of metals and alloys including iron¹⁵⁻¹⁷, stainless steels¹⁸⁻²³ and aluminum²⁴⁻²⁸. Furthermore, many of these publications have established, using potentiodynamic methods, that a simple logarithmic relationship exists between E_b and $[Cl^-]$, given by the following,

$$E_b = A + B \log_{10} [Cl^-] \quad (1)$$

where A and B are constants which depend on factors such as the type of metal or alloy and on the composition of the corrosive electrolyte. Typically, E_b is established potentiodynamically, whereby a positive-going sweep of potential applied to the passive metal is carried out and E_b is identified at a point in the passive region where a sharp rise in

current density is encountered. The origin of this dependence has been ascribed both to a model involving transport phenomena inside corrosion pits¹⁵ and the point-defect model of breakdown in metal oxide passive films^{17,21,22,29}. Given the apparent temporary passive behavior and subsequent breakdown of passivity observed previously for Mg in chloride-containing aqueous solutions¹⁰⁻¹⁴, a possible dependence of E_b on $[Cl^-]$ would be anticipated.

Several authors have already investigated the influence of chloride ion concentration and pH on the corrosion behavior of various Mg alloys using a combination of anodic polarization and electrochemical impedance spectroscopy^{30 - 33}. However, although the general consensus from these works is that increasing chloride concentration ($[Cl^-]$) leads to higher rates of corrosion, a well-defined relationship between corrosion resistance and $[Cl^-]$ has yet to be determined. In addition, polarization curves presented by these authors^{30 - 33} and as part of other investigations¹¹ suggest that under certain conditions of pH and $[Cl^-]$, Mg and its alloys display a well-developed passive region along with clearly discernible trans-passive behavior. In this work we use a combination of conventional potentiodynamic experiments and a new method of establishing E_b , by monitoring time-dependent free corrosion potential behavior, to demonstrate that passivity and its chloride-induced breakdown plays a pivotal role in the corrosion behavior of Mg. The pre- and post-breakdown localized corrosion characteristics of specimens comprising two different iron impurity levels of 40 (high purity, HP) and 280 ppm (commercial purity, CP) are investigated under conditions of varying pH and chloride ion concentration. Herein we set out to investigate whether a relationship exists between the potential at which Mg passivity breakdown occurs and the chloride ion concentration of the immersion electrolyte. In so doing we demonstrate a robust method of establishing E_b under circumstances where breakdown occurs in the absence of external polarization. We also show that conventional potentiodynamic methods may also be employed to determine E_b in situations where sustained passivity is observed in freely corroding conditions.

2. Experimental Details

Materials: Two different types of pure magnesium were studied in this work. Commercial purity (CP) magnesium foil (99.9+%, 1 mm thickness) was obtained from Goodfellow Metals Ltd, with the main impurities being iron (280 ppm) and manganese (170 ppm). A high purity (HP) magnesium (99.99%) specimen, with principal impurity elements being Fe (40 ppm), Ni

(10 ppm) and Cu (20 ppm), characterized in previous work^{13, 34}, was also studied for comparative purposes. Specimens of AZ31 alloy, prepared from an as-cast ingot of composition 3.1% Al, 0.7% Zn, 0.24% Mn (all % w/w) with balance Mg, was supplied by Magnesium Elektron Ltd. In all cases, flat coupons were abrasively cleaned using an aqueous slurry of 5 μm polishing alumina, washed with aqueous surfactant and rinsed with distilled water followed by ethanol. Samples for SVET immersion experiments were then prepared by covering the surface with 90 μm thick extruded PTFE 5490 tape (3M Ltd), such that only a 6 \times 6 mm square area in the centre of one face was exposed to electrolyte. All electrolytes were prepared using analytical grade reagents (Aldrich Chemical Co.) and distilled water. Solution pH was adjusted to the required value by the dropwise addition of either HCl (aq) or NaOH (aq). In the case of specimens employed for potentiodynamic experiments, electrical wire contact was made by means of a conductive silver paste, and the samples were subsequently cold mounted in two-part epoxy resin so that one face was exposed. The upper surface was then covered with PTFE tape so that only a 6 \times 6 mm square area remained exposed.

Methods: Scanning vibrating electrode measurements were carried out using a probe comprising a 125 μm diameter platinum micro-disc probe prepared by sealing Pt wire in a glass sheath. The probe vibration frequency was 140 Hz and the peak-to-peak vibration amplitude (A_{pp}), as measured stroboscopically in air was $\pm 20 \mu\text{m}$. Movement of the SVET probe-vibrator assembly was achieved using three orthogonal linear bearings driven by stepper motors (Time and Precision Ltd). The SVET voltage signal was detected using a Perkin Elmer 7265 lock-in amplifier and subject to digital signal averaging (typically of 10 successive measurements) to further enhance signal-to-noise ratio. By Ohm's law, the peak-to-peak SVET voltage signal (V_{pp}) is related to current flux density along the axis of probe vibration (j_z) by,

$$V_{pp} = j_z (A_{pp}/\kappa) \quad (2)$$

where κ is solution conductivity, such that a quantity $G = \kappa/A_{pp}$ may be defined as the SVET calibration factor. The SVET calibration was checked galvanostatically in aqueous NaCl electrolyte of different concentration using a specially devised two-compartment cell and a nano-galvanostat of in-house design described in detail previously¹⁰. At an electrolyte

concentration of 1 mol dm^{-3} NaCl (aq) and for $j_z = -100 \text{ A m}^{-2}$ to $+100 \text{ A m}^{-2}$, plots of V_{pp} versus j_z gave a good straight lines (correl. coeff. > 0.998) and the values of G obtained from plot gradients agreed with those calculated using equation (2) to within $\pm 10\%$.

Magnesium samples were completely immersed, exposed area uppermost, in an electrolyte bath containing aqueous sodium chloride solution at the required pH. The bath was left unstirred and in contact with room air at a nominal temperature of 20°C . The SVET probe was held vertically and scanned at a fixed height ($100 \mu\text{m}$) above the metal surface. Samples were scanned immediately following immersion, and continuously thereafter for a period of up to 100 minutes. Each scan took *ca.* 6 minutes and produced a square matrix of 900 V_{pp} data points. Individual V_{pp} values were converted to j_z , using the relevant calibration factor G . A more comprehensive description of the SVET apparatus employed in this work is given elsewhere^{10, 23}. Studies of time dependent free corrosion potential (E_{corr}), along with potentiodynamic experiments in electrolytes containing varying sodium chloride concentration were carried out using a Solartron 1280B workstation in conjunction with a conventional 3 cell arrangement. This consisted of a Pt gauze counter electrode and saturated calomel (SCE) reference electrode using a Luggin capillary to minimize any ohmic drops possible when using dilute chloride concentrations. For measurements carried out using a solution pH of 11, the NaCl (aq) electrolyte was purged for 10 min using synthetic air prior to experimentation to ensure that any influence due to dissolved carbon dioxide from the atmosphere was minimised.

3. Results and Discussion

3.1 Passivity breakdown in commercial purity magnesium (CP-Mg)

Figure 1 shows typical behavior of CP-Mg specimens when subjected to potentiodynamic polarization in electrolytes containing varying concentrations of sodium chloride at pH 7. The figure shows that chloride ion concentration has relatively little effect on cathodic behavior, where the majority of j vs E curves presented can be superimposed. However as chloride ion concentration is decreased from 1 to $0.005 \text{ mol dm}^{-3}$ (curves i to v), an obvious shift in open circuit potentials to more positive values is observed and the magnitude of anodic current density falls significantly over the same range of applied potential. Nevertheless, the

polarization curves show no evidence of passivity breakdown, typified by the presence of a passive region in the anodic branch and breakdown characterized by a sharp increase in j with E , and no meaningful information regarding the influence of chloride ion concentration on passivity breakdown can be obtained. However, previously published work has demonstrated that monitoring time-dependent free corrosion potentials can provide a means of establishing an apparent breakdown potential (E_b) under circumstances where the Mg specimen undergoes spontaneous breakdown in the absence of external polarization^{10, 35}. Figure 2 (a) shows the variation of free corrosion potential (E_{corr}) with time over the first hour of immersion for a CP-Mg specimen in 1 mol dm^{-3} NaCl (aq) at pH 7. Also included in Figure 2 (b – d) is a series of close-up images of the corroding Mg surface, showing visual appearance correlated with time-dependent E_{corr} values. In addition, SVET-derived current density distribution maps, obtained at the same immersion times, are also provided in Fig 2 (b – d) to again correlate with time-dependent E_{corr} measurements and help in explaining the observed E_{corr} vs time relationship.

Prior to any visual evidence of breakdown, Fig 2 (a) shows that E_{corr} rises rapidly with time over several minutes from a starting value of -1.7 V up to a point where E_{corr} exceeds the apparent breakdown potential (E_b) of -1.625 V vs. SCE. At the point of breakdown E_{corr} drops significantly (by ca. 40 mV from its maximum value), attaining a constant value of -1.665 V vs. SCE after 6-8 min immersion. During the period where E_{corr} is seen to rise following initial immersion, the polished Mg surface rapidly acquires a cloudy white surface film. Film formation is accompanied by the appearance of hydrogen bubbles at several points over the surface of the exposed metal. However at the point of maximum E_{corr} , a dark circular spot appears on the exposed metal, indicated by the arrow on the photographic image in Fig 2 (b), from which a rising stream of hydrogen gas is evolved. The accompanying SVET-derived j_z surface map, also shown in Fig 2 (b), reveals the point of breakdown to be a region of intense local anodic activity. The relaxation in E_{corr} coincides with a period where the initial dark spot expands in a radial manner. Figure 2 (c) shows a typical image confirming that the diameter of the original dark spot had increased significantly with immersion time. A representative j_z map recorded at the same immersion time, shows that as the corrosion disc expands radially, intense local anodic activity is maintained around its circumference, while the interior becomes strongly cathodic. Any localized corrosion currents emerging from the intact, film covered Mg surface remain negligible by comparison. However, as post-breakdown corrosion develops and a progressively greater proportion of the intact, film-

covered Mg is converted into a dark, roughened surface, E_{corr} subsequently rises and eventually exceeds the original E_{corr} maximum observed at the point of breakdown. Figure 2 (d) shows the appearance of the working electrode surface at this juncture, while the associated SVET-derived j_z map confirms that the majority of the exposed surface has become cathodically activated, although an intense local anode persists at the boundary of the corroded and intact Mg regions.

An SVET-derived surface map of current density (j_z) obtained during the initial stages of Mg corrosion ($t < 6$ min) can be used to explain the local electrochemical events underlying the observed rapid rise in time-dependent E_{corr} immediately upon immersion and over the subsequent time period prior to breakdown (Figure 3). In the early stages of immersion in chloride containing electrolyte, an imperfect film of magnesium (hydr)oxide is formed on the exposed magnesium surface. When Mg^{2+} ions, formed by the anodic dissolution of magnesium via reaction (3),



encounter an elevated pH caused by cathodic hydrogen evolution (reaction (4)), then a film of $\text{Mg}(\text{OH})_2$ will form at regions on the exposed surface where local concentrations of Mg^{2+} and OH^- are sufficiently high that the solubility product of $\text{Mg}(\text{OH})_2$ is exceeded. It is evident that localised corrosion plays a role in the growth of a surface hydroxide film, where a distributed anode located on the left hand side of the working electrode area in Figure 3 ($j_z = \text{ca } 2 \text{ A m}^{-2}$) appears to be galvanically coupling with several focal areas of cathodic activity at “pinholes” of exposed Mg on an otherwise film-covered surface. These cathodically active regions coincide with points on the intact Mg surface where H_2 bubbles are slowly evolved. Upon closer inspection of film covered Mg areas which remain distant from the expanding corrosion “disc”, it appears that the activity of these focal cathodic regions decrease with time, falling by up to 80% over a 30 min immersion period from initial values in the range -4 to -16 A m^{-2} . From the local anodic current density of $+2 \text{ A m}^{-2}$ which SVET initially detects over a significant proportion of the exposed Mg surface, a surface film growth rate of 0.25 nm s^{-1} may be calculated, assuming that the film is composed solely of $\text{Mg}(\text{OH})_2$ (density =

2.37 g cm⁻³)³⁶. It seems plausible therefore to conclude that SVET-detectable localized currents play a major role in the build-up of a semi-protective surface hydroxide film prior to breakdown.

Based on SVET-derived data obtained prior to breakdown, the schematic diagram given in Figure 4 demonstrates how a Mg(OH)₂ film is formed on the exposed surface as a result of localized, pre-breakdown corrosion activity. It is well known that iron-rich second-phase particles constitute the principal cathodic hydrogen evolution reaction site on Mg^{37, 38}. Reaction (4) is shown to be highly focused on just a few points on the exposed surface, which probably coincide with the location of a high number density of iron-rich impurity phases which break the surface at these points. The rise in E_{corr} observed when a Mg specimen is initially immersed in chloride electrolyte is explained by a progressive thickening of the (hydr)oxide film, shown schematically in Fig 4, leading in turn to anodic deactivation. According to mixed potential theory, electro-neutrality will be maintained when the specimen adopts a more positive potential, which in turn (as observed by SVET) leads to a suppression of local cathode current density values. The rise in E_{corr} from initial immersion at t_1 will continue up to the point where it becomes equal to or exceeds the value of E_b (at t_2) whereupon highly localized Mg dissolution of the Mg occurs and a significantly higher rate of localized corrosion ensues^{10, 11}. The sharp drop in E_{corr} immediately following the point of breakdown may be understood again in terms of mixed potential theory. The significant increase in anodic current, shown to emerge solely from a location which coincided with the appearance of a black corrosion spot on the exposed surface, will cause the Mg potential to become more negative in order to increase the corresponding cathodic current and maintain electroneutrality. It should be noted that despite the decrease in E_{corr} , no passivation of the local anode is observed. This is because the site of initial anodic attack becomes strongly cathodically activated, eventually producing an intense local cathode (see Figures 2c and d) which sustains radial growth of the anodic region. Eventually however, at a point where over half of exposed area is occupied by a dark, cathodically activated corroded surface (see Fig 4d), E_{corr} rises with time once again, in this case to compensate for the progressive growth in local cathode area.

3.2 Chloride ion concentration effects on time-dependent E_{corr} behavior.

Having established that monitoring an inflection in E_{corr} versus time plots can conveniently indicate a breakdown potential for Mg, further experiments were carried out over a range of sodium chloride concentrations in order to establish whether E_b is significantly influenced by chloride ion concentration. Figure 5 shows a comparison of typical E_{corr} vs. time curves obtained for CP-Mg immersed in NaCl (aq) at pH 7 over a 0.005 to 2.5 mol dm⁻³ concentration range. The series of curves given in Fig 5 clearly shows a significant effect of chloride ion concentration on time-dependent E_{corr} characteristics, where the value of E_b (marked by maxima in E_{corr} vs t curves) becomes progressively promoted to more positive potentials with decreasing [Cl⁻]. Another consequence of a progressive decrease in [Cl⁻] is that the time taken for breakdown to occur lengthens considerably, from 1 min to ca. 20 min as [Cl⁻] is reduced from 2.5 to 0.01 mol dm⁻³. When immersed in 0.005 mol dm⁻³ NaCl (aq) at an initial pH of 7, no evidence of CP-Mg breakdown was observed for up to 60 min immersion. Interestingly, the E_{corr} versus time curves for all chloride ion concentrations appear to overlay each other up to the point that breakdown occurs. This implies that the electrochemical processes responsible for the initial rapid rise in E_{corr} , as represented by the scheme given in Fig 4 are largely independent of [Cl⁻]. If this is indeed the case, then it seems that there is sufficient conductivity present, even in the least concentrated chloride electrolyte of 5 × 10⁻³ mol dm⁻³ employed here, to permit highly localised cathodic regions to couple with larger weakly anodic areas over significant distances of 1 mm or greater.

However, following the point of passivity breakdown, marked by a rapid drop in E_{corr} from an apparent maximum value corresponding to E_b , there is a more apparent influence of chloride ion concentration. As discussed previously, a progressive decrease in [Cl⁻] causes the maximum value of E_{corr} observed before breakdown to increase, with a span of ca 300 mV observed at the extremes of the concentration range studied. In addition, the extent to which E_{corr} decreases from its maximum appears to vary from ca. 10 – 20 mV, seen at the extremes of the [Cl⁻] range (see Fig 5 curves i and vi), to significantly greater changes of ca. 50 – 70 mV observed at intermediate concentrations. The smaller drop in time-dependent E_{corr} observed at dilute concentrations may be understood in terms of significantly lower anodic j_z values observed at the location(s) of Mg breakdown^{10, 14}, compared to values measured at higher [Cl⁻]. However, the relatively small relaxation in E_{corr} observed at [Cl⁻] = 2.5 mol dm⁻³ is less readily explained on this basis and further work is required to clarify this apparent anomalous behavior.

Values of E_b established from the various E_{corr} vs time curves given in Fig 5 were subsequently plotted as a function of chloride ion concentration (see Figure 6) and showed a clear dependence on $[\text{Cl}^-]$ according to the equation (1) shown previously in Section 1. Each value of E_b represents the average value of 3 separate immersion experiments. Under the conditions used for these experiments, values of -1.63 V and -0.11 V/decade were obtained for A and B respectively for CP-Mg. The value of A equates to the magnitude of E_b established at a chloride ion concentration of 1 mol dm^{-3} . The obvious dependence of E_b on $\log_{10}[\text{Cl}^-]$ was observed over a one and a half order of magnitude concentration range (0.1 to 2.5 mol dm^{-3}), but deviated from this relationship at more dilute concentrations of $\leq 0.02 \text{ mol dm}^{-3}$. Figure 6 also includes E_b vs $[\text{Cl}^-]$ data obtained in a separate set of immersion experiments carried out at an elevated starting pH of 11 (see circular data point markers). The excellent agreement of the values of A and B with results obtained at a lower starting pH confirms that for this highly impure form of Mg, resistance to passivity breakdown cannot be obtained by simply raising the solution pH.

Identical experiments were also carried out using a technologically important alloy, namely AZ31, which also undergoes apparent breakdown of temporary passivity over a range of chloride ion concentration in the absence of external polarisation¹³. Previous studies using in-situ SVET analysis of unpolarised AZ31 showed again that passivity breakdown locations coincided with intense focal net anodes which once initiated, proceeded to traverse the intact un-corroded AZ31 surface and produce a cathodically-activated corroded surface. A typical family of E_{corr} vs time curves obtained over the same $[\text{Cl}^-]$ range studied previously for CP-Mg is shown in Figure 7a. Although the E_{corr} inflections are generally less pronounced compared to those observed for CP-Mg, the maxima corresponding to the point of breakdown are discernible and show a clear trend of increasing E_b with a progressive decrease of $[\text{Cl}^-]$. Again, breakdown was observed within a few tens of seconds following immersion in the most concentrated test electrolyte, increasing to $> 100 \text{ s}$ at more dilute chloride concentrations. However, the clear trend of increased time to breakdown with decreasing $[\text{Cl}^-]$ observed for CP-Mg was not so evident in the case of AZ31. A corresponding plot of E_b versus $\log_{10}[\text{Cl}^-]$, obtained from the mean of 3 separate immersion experiments at each

chloride concentration, is given in Figure 7b. Again the plot shows a straight line relationship over a 2 order of magnitude $[Cl^-]$ range, where $A = -1.59$ V and $B = -0.072$ V/decade.

A dependence of breakdown potential on chloride ion concentration, determined by anodic polarization experiments on both AZ31 and AZ91 alloys has been reported elsewhere^{30, 31}, although not described mathematically by the authors. From the data presented therein, values of E_b were identified from inflections in anodic branch polarization curves, which indicate apparent passive to trans-passive behaviour. A re-working of this data for comparative purposes gave E_b versus $\log_{10}[Cl^-]$ slopes of -0.14 and -0.125 V per decade for AZ91³⁰ and AZ31³¹ respectively. Although the magnitudes of B from these replotted datasets appear higher than the values established in this work for CP-Mg and AZ31, they nevertheless demonstrate that the same \log_{10} dependence can be observed when determining E_b by an alternative method.

3.3 Chloride ion concentration effects on high purity (HP) Mg passivity breakdown

To further test the assertion that a potentiodynamic method could also be used to establish an apparent breakdown potential in Mg, a separate investigation was carried out using high purity (HP) Mg specimens, comprising a significantly lower iron impurity content. Previous studies have shown that this type of Mg can also undergo spontaneous breakdown when immersed in concentrated chloride-containing electrolyte in the absence of external polarisation¹¹. However, subsequent propagation of filiform-like corrosion is observed on the post-breakdown surface, rather than disc-form localized corrosion obtained for CP-Mg in 1 mol dm^{-3} NaCl (aq) at pH 7^{10, 14}. Again, polarization curves carried out using different concentrations of NaCl (aq) electrolyte at pH 7 showed no obvious evidence of passive to trans-passive behavior as shown in Figure 8a. As in the case of the CP-Mg discussed previously, a decrease in $[Cl^-]$ produced the greatest effect on the anodic branches of curves i – iv, although no significant shift in open circuit potential was observed. A study of E_{corr} versus time behavior as a means of identifying E_b , under conditions where spontaneous breakdown can occur, proved less successful than for the case of a more impure form of Mg described previously in section 3.2. This was largely due to the rather protracted times observed for the HP-specimens to break down, especially at $[Cl^-] < 0.1 \text{ mol dm}^{-3}$. In addition,

the obvious inflection in E_{corr} versus time curves were less apparent for HP-Mg, where only small decreases in E_{corr} of typically a few mV were observed at the point of breakdown, making the maximum value of E_{corr} ($=E_b$) difficult to establish. This, in turn probably derives from the significantly lower local anodic current density values measured for HP-Mg at the locations of focal breakdown, typically $+50$ to $+100 \text{ A m}^{-2}$ measured at part of a separate investigation¹⁴, when compared with values of $+250 \text{ A m}^{-2}$ observed for CP-Mg under the same conditions¹⁰.

As a result, a more conventional potentiodynamic means of identifying E_b was employed, using an elevated pH of 11, where HP-Mg was shown to remain passive in chloride-containing electrolytes at all concentrations of 2 mol dm^{-3} or lower for immersion periods of many hours. Typical polarization curves observed for HP-Mg in pH 11 electrolyte containing varying sodium chloride concentrations over 3 orders of magnitude are given in Figure 8b. To avoid any potential interference from carbonate anions derived from dissolved ambient carbon dioxide, each solution was sparged for 10 min using synthetic air prior to each potential sweep. At elevated pH a clear inflection in the anodic branches of curves ii – vi was observed in Fig 8b, signifying passivity breakdown and trans-passive behaviour shown as a rapid increase in anodic current density with applied potential. This indication of passivity breakdown in the anodic branches of the polarization curves also becomes progressively well-developed as $[\text{Cl}^-]$ is decreased. The potential at which the inflection was observed was used as the value of breakdown potential E_b . Average values of breakdown potential (E_b), taken at the point of sharp inflection in anodic polarization curves for multiple repeat experiments, showed a clear dependence on $[\text{Cl}^-]$ (see Figure 9, line i), according to the relationship, given previously in equation (4).

Under the conditions used for these experiments, values of -1.60 V and -0.11 V/decade were obtained for A and B respectively for HP-Mg. The value of B is identical to the value previously determined for CP-Mg at pH 7, albeit by a method involving monitoring time-dependent E_{corr} behaviour. Also shown in Figure 9 is a plot of E_{corr} versus $[\text{Cl}^-]$, established over 10 min immersion prior to the start of a potentiodynamic sweep in a given NaCl (aq) electrolyte at pH 11. E_{corr} is shown to become more negative with increasing $[\text{Cl}^-]$, albeit with a significantly shallower gradient of -0.03 V/decade . The point at which the 2

plots intersect, indicated by the arrow in Fig. 9, represents the threshold $[Cl^-]$ at which $E_{corr} = E_b$ and spontaneous breakdown in the absence of external polarization would be expected. For the HP-Mg studied here at pH 11, this threshold is at a chloride ion concentration 8 mol dm^{-3} , i.e. higher than the $[Cl^-]$ of a saturated NaCl (aq) solution at room temperature.

3.4 The origin of the logarithmic dependence of E_b on $[Cl^-]$

An important question to address concerns the origin of E_b dependence upon $\log_{10}[Cl^-]$ observed for Mg, demonstrated by both monitoring E_{corr} transient behaviour and via a potentiodynamic method. Published theories for other metals such as Al, Fe and Ni explain the $[Cl^-]$ dependence of E_b as per equation (1) either on the basis of transport processes within a corrosion pit¹⁵, or the breakdown of a passive oxide surface film according to the point defect model^{17,21,29}. In the former, Galvele considered the breakdown potential to represent the minimum potential at which localized acidity could be maintained inside a pit¹⁵. Consequently the E_b vs $[Cl^-]$ relationship was derived from a model which assumed that the bulk solution containing aggressive chloride anions acted as a supporting electrolyte for anodic metal dissolution ($M \rightarrow M^{n+} + ne^-$) occurring exclusively at the base of a pit, coupled with subsequent metal cation (M^{n+}) hydrolysis inside the pit according to the following equation.



By calculating concentrations of M^{n+} , Na^+ , Cl^- and electrical potential inside the pit as a function of the product of pit current and depth, a logarithmic dependence of the potential change with $[Cl^-]$ was predicted. In contrast, Macdonald's point defect model^{17,21,29} derives the same relationship of E_b with $[Cl^-]$ by considering the effect of Cl^- absorption into surface oxygen vacancies of a passive metal oxide film. This, in turn is proposed to catalyse the formation of cation vacancies at the solution/film interface and increase the rate of their movement towards the metal/oxide film interface. Here, they may either become annihilated by cation injection from the substrate metal or accumulate if the cation vacancy flux is sufficiently high. At a point where the rate of accumulation exceeds a critical value,

separation of the oxide film from the underlying metal will occur and as a consequence of continued dissolution at the solution/film interface, a local thinning of the passive film eventually causes breakdown and pit initiation.

For metals such as Al and Fe, the 1st hydrolysis equilibrium constants for equation (5) (pK_a^1) are 5.0 and 2.2 respectively³⁶, signifying that Al^{3+} cations are moderately acidic, while Fe^{3+} strongly acidifies in aqueous solution. Thus it can be envisaged how the Galvele model, developed using ion transport conditions which will maintain a critical low pH value inside a pit, will apply to these metals. However, in contrast the pK_a^1 value for Mg is 11.4³⁹, signifying that Mg^{2+} cations are non-acidic in aqueous solution and would not be anticipated to generate a low pH within a pit-like environment. The observation that a E_b vs $\log_{10}[\text{Cl}^-]$ relationship exists for Mg, is therefore not consistent with the Galvele approach¹⁵ and suggests that the observed chloride ion concentration dependence of E_b is probably best explained on the basis of the point defect model²⁹. In support of this, it should be noted that the existence of a pit-like feature on Mg immediately following breakdown is only temporary and within seconds a combination of a local increase in pH coupled with cathodic activation of the previously anodically attacked surface causes the anode to move from its original initiation location. In addition, the Cl^- -catalysed thinning of the passive oxide film, postulated by point defect model, can also be explained on the basis of a chemical interaction, where previous studies have confirmed a significant influence of $[\text{Cl}^-]$ on the solubility of $\text{Mg}(\text{OH})_2$ ³⁹. This study demonstrated that the solubility product (K_{sp}) of $\text{Mg}(\text{OH})_2$ varied with chloride ion concentration in the range $10^{-2} - 1 \text{ mol dm}^{-3}$ according to the following expression,

$$K_{\text{sp}} = K_{\text{sp}}^1 + 4.8 \times 10^{-11} \log_{10}[\text{Cl}^-] \quad (6)$$

where $K_{\text{sp}}^1 = 1.24 \times 10^{-11} \text{ mol}^3 \text{ dm}^{-9}$, i.e. the measured solubility product in $1 \text{ mol dm}^{-3} \text{ NaCl (aq)}$ ³⁹. Therefore, in the NaCl concentration range used for this work, it can be shown that K_{sp} increases by up to a factor of 4 compared to a situation where no chloride is present. Previous ex-situ studies of the composition of Mg surface films formed in unpolarised NaCl(aq) ⁴⁰ showed the presence of magnesium chlorides and hydroxy-chlorides within the $\text{Mg}(\text{OH})_2$ layer, indicating that incorporation of Cl^- may be a precursor to film breakdown. It

is likely therefore that breakdown occurs at a weak point in the surface film, where Cl^- migration and accumulation has led to a thinning of the protective Mg(hydr)oxide layer. A note of caution should however be exercised in comparing the behaviour of passive films formed on stainless steel and aluminium with the apparently temporarily protective surface films formed on pure Mg. Several studies have shown that under aqueous immersion conditions a complex duplex surface film is formed comprising an inner MgO and an outer $\text{Mg}(\text{OH})_2$ layer⁴¹⁻⁴⁴, whose combined thickness is considerably greater than that of passive film thicknesses of < 6 nm typically determined for 304 grade stainless steel⁴⁵ or aluminium⁴⁶. Nevertheless, short immersion times (< 5 min) are reported to produce an inner MgO layer thickness of the order of 2.5 nm⁴³, and as such it may be possible to draw comparisons with passive film breakdown on other metals. In so doing, this would necessarily imply that chloride-induced local thinning of this inner MgO layer is the most important precursor to breakdown, although this would also be contentious given the findings of others⁴⁴ who report that the outer $\text{Mg}(\text{OH})_2$ is the least porous of the two layers.

A final consideration should be given to the practical implications of the existence of a distinct breakdown potential for Mg and its alloys and the observed chloride ion concentration dependence of E_b . The work described herein has demonstrated that Mg breakdown will only occur above a threshold electrolyte ($[\text{Cl}^-]_b$) which lowers E_b to a point where E_{corr} adopted in the absence external polarisation becomes $\geq E_b$. If $[\text{Cl}^-]$ is below this threshold concentration for spontaneous breakdown, then passivity is sustained indefinitely. For example, when bulk corrosion rates for CP-Mg immersed in NaCl (aq) electrolytes of varying concentrations were determined by time-dependent volumetric hydrogen measurements, the rate measured at $[\text{Cl}^-] = 10^{-3} \text{ mol dm}^{-3}$, where breakdown did not occur, was negligible compared with rates established at higher $[\text{Cl}^-]$. This is shown in the plots of mol H_2 evolved as a function of immersion time given in Figure 10, where breakdown and the subsequent evolution of a dark corroded surface were observed at all $[\text{Cl}^-] \geq 10^{-2} \text{ mol dm}^{-3}$ (see Fig 10, plots i, ii and iii). The large difference in the post-breakdown corrosion rate of $0.003 \text{ mol H}_2 \text{ min}^{-1}$ measured at $[\text{Cl}^-] = 10^{-2} \text{ mol dm}^{-3}$, compared to the rates of ca $0.042 \text{ mol H}_2 \text{ min}^{-1}$ measured at both 0.1 and 1 mol dm^{-3} NaCl (aq), is due to the propagation of ohmically-controlled filiform-like corrosion in the latter case¹⁴, while surface controlled disc-form corrosion is observed at the two higher $[\text{Cl}^-]$ employed.

Therefore, it seems that to gain an accurate picture of Mg alloy corrosion rates in immersion tests, a judicious selection of test solution $[\text{Cl}^-]$ should be made to avoid a

situation where breakdown does not occur, giving in turn an artificially low rate of corrosion. The use of a sufficiently high $[\text{Cl}^-]$ to exceed the threshold concentration for spontaneous breakdown, leading to propagation of localised corrosion feature would have certainly produced a significantly higher bulk rate of corrosion along with entirely different conclusions regarding the corrosion resistance of the test piece.

4. Conclusions

A simple method of determining a breakdown potential (E_b) for Mg surfaces which undergo spontaneous breakdown and ensuing localized corrosion propagation in the absence of external polarization was demonstrated. The method involved monitoring time-dependent free corrosion (E_{corr}) potential changes, where breakdown was characterized by an E_{corr} maximum followed by a rapid relaxation of potential to more negative values. E_b values were measured as a function of $[\text{Cl}^-]$ for both commercial purity Mg and AZ31 alloy specimens immersed in aqueous sodium chloride electrolytes at pH 7 and shown obey the relationship $E_b = A + B \log_{10} [\text{Cl}^-]$, where A and B are constants. An identical chloride ion concentration dependence of E_b was demonstrated for high purity magnesium at pH 11 using a potentiodynamic method, where clear evidence of passivity breakdown in the anodic branches of the family of polarization curves is observed. The same value of B (- 0.11 V /decade) was determined for Mg using both methods of establishing E_b and apparently independent of the impurity level in the specimens. It is proposed that the relationship of E_b with $[\text{Cl}^-]$ derives in part from the chloride ion influence on the solubility product (K_{sp}) of magnesium hydroxide, where K_{sp} is known to be a function of $\log_{10} [\text{Cl}^-]$. From the literature explanations of the E_b vs $\log_{10} [\text{Cl}^-]$ relationship observed for other metals, it would seem that the point defect model best represents Cl^- -induced Mg passivity breakdown, since the non-acidic nature of the Mg^{2+} cation is inconsistent with assumption of low pH within pits made by alternative theories.

Acknowledgements: The College of Engineering, Swansea University is thanked for providing funding for a post-doctoral position for Hefin Dafydd.

Figure Legends

Figure 1: Anodic-going potentiodynamic polarisation curves obtained for CP-Mg in electrolytes consisting of, i. 1, ii. 0.2, iii. 0.05, iv. 0.02 and v. 0.005 mol dm⁻³ NaCl (aq) at pH 7 in aerated conditions at room temperature. A sweep rate of 1 mV s⁻¹ was employed in each case.

Figure 2: Time-dependent E_{corr} variation (a) observed for CP-Mg upon immersion in 1 mol dm⁻³ NaCl (aq) at pH 7, correlated with both photographic images and SVET-derived current density distribution maps of the corroding surface obtained at intervals of (b) 3 min, (c) 20 min and (d) 40 min following initial immersion.

Figure 3: Surface map showing the distribution of current density (j_z) above a CP-Mg sample immediately following immersion in aerated 1 mol dm⁻³ NaCl (aq) at pH 7, but prior to breakdown.

Figure 4: Schematic representation of localized corrosion activity on CP-Mg upon initial immersion, leading to the observed time-dependent rise in E_{corr} .

Figure 5: Plots of E_{corr} versus time obtained for CP-Mg specimens immersed in neutral, aerated NaCl (aq) electrolyte at concentrations of, i. 2.5, ii. 1.0, iii. 0.2, iv. 0.1, v. 0.05, vi. 0.02, vii. 0.01 and viii. 0.005 mol dm⁻³.

Figure 6: Summary plot of breakdown potential (E_b) versus chloride ion concentration established for CP-Mg samples at pH 7 in aqueous NaCl (aq) electrolyte. The circular data points represent results obtained using the same chloride ion concentrations but at an elevated pH of 11.

Figure 7: Plots of (a) E_{corr} versus time obtained for AZ31 alloy specimens immersed in neutral, aerated NaCl (aq) electrolyte at concentrations of, i. 5, ii. 1, iii. 0.2, iv. 0.05, v. 0.01, and vi. 0.005 mol dm⁻³ along with (b), a summary plot of breakdown potential (E_b) versus chloride ion concentration.

Figure 8: Anodic-going potentiodynamic polarisation curves obtained at (a) pH 7 and (b) pH 11 for HP-Mg in electrolytes comprising different chloride ion concentrations. In both cases of $[Cl^-] =$ i. 2, ii. 0.5, iii. 0.1 and iv. 0.02 mol dm^{-3} NaCl (aq), while for (b) only curves v and vi were obtained using concentrations of 0.005 and $0.002 \text{ mol dm}^{-3}$ NaCl respectively. A sweep rate of 1 mV s^{-1} was employed in each case.

Figure 9: Summary plot of (i) breakdown potential (E_b) and (ii) free corrosion potential (E_{corr}) versus chloride ion concentration obtained for HP-Mg in NaCl-containing electrolyte at pH 11.

Figure 10: Plots of moles hydrogen gas per unit area evolved versus time for CP-Mg immersed under freely corroding conditions in (i) 1, (ii) 0.1, (iii) 0.01 and (iv) $10^{-3} \text{ mol dm}^{-3}$ NaCl (aq) at pH 7.

References

1. G.L. Makar, J. Kruger, *Int. Mater. Rev.*, 38 (1993): p. 138.
2. G. Song, A. Atrens, *Adv. Eng. Mater.*, 1 (1999): p. 11.
3. G. Song, A. Atrens, *Adv. Eng. Mater.*, 5 (2003): p. 837
4. E. Ghali, W. Dietzel, K.U. Kainer, *J. Mater. Eng. Perf.*, 13 (2004): p. 7.
5. G. Song, *Adv. Eng. Mater.*, 7 (2005): p. 563.
6. R. Zeng, J. Zhang, W. Huang, W. Dietzel, K.U. Kainer, C. Blawert, K.E. Wei, *Trans. Nonferrous Met. Soc. Chi.*, 16 (2006): p. s763.
7. E. Ghali, *Corrosion resistance of Aluminium and Magnesium alloys*, John Wiley and Sons, New Jersey USA, (2010).
8. N.T. Kirkland, N. Birbilis, M.P. Staiger, *Acta Biomaterialia*, 8 (2012): p. 925.
9. Z. Szklarska-Smialowska, *Pitting and Crevice Corrosion*, NACE International, Houston, TX (2005).

10. G. Williams and H.N. McMurray, *J. Electrochem. Soc.*, 155 (2008): p. B340.
11. K.D. Ralston, G. Williams and N. Birbilis, *Corrosion*, 68 (2012): p. 507.
12. G. Williams, R. Grace, *Electrochimica Acta*, 56 (2011): p. 1894.
13. G. Williams, H. Ap Llwyd Dafydd, R. Grace, *Electrochimica Acta* 109 (2013): p. 489.
14. G. Williams, N. Birbilis, H.N. McMurray, *Faraday Discussions*, 180, (2015): p. 313.
15. J. Galvele, *J. Electrochem. Soc.*, 123 (1976): p. 464
16. M. Alvarez, J. Galvele, *Corros. Sci.*, 24 (1984): p. 27
17. S. Sharifi-Asla, F. Mao, P Lu, B. Kursten, D.D. Macdonald, *Corros. Sci.*, 98 (2015): p. 708.
18. H.P. Leckie, H.H. Uhlig, *J. Electrochem. Soc.* 113 (1966): p. 1,262.
19. J.-H. Wang, C.C. Su, Z. Szklarska-Smialowska, *Corrosion* 44 (1988): p. 732.
20. N.J. Laycock, R.C. Newman, *Corros. Sci.* 40 (1998): p. 887.
21. Y. Zhang, D.D. Macdonald, M. Urquidi-Macdonald, G. R. Engelhardt, R.B. Dooley, *Corros. Sci.* 48 (2006): p. 3812.
22. C.B. Breslin, D.D. Macdonald, J. Sikora, E. Sikora, *Electrochimica Acta*, 42, (1997): p. 127.
23. G. Williams, H.N. McMurray, *Corrosion*, 62 (2006): p. 231
24. H. Böhni and H. H. Uhlig, *J. Electrochem. Soc.*, 116 (1969): p. 906
25. S. T. Pride, J. R. Scully and J. L. Hudson, *J. Electrochem. Soc.*, 141 (1994): p. 3028
26. E. McCafferty, *Corros. Sci.*, 37 (1995): p. 481
27. E. McCafferty, *Corros. Sci.* 45 (2003): p. 1421
28. J. Soltis, N.J. Laycock and D. Krouse, *Corros. Sci.* 53 (2011): p. 7
29. D.D. Macdonald, *J. Electrochem. Soc.*, 139 (1992): p. 3434.
30. F. El-Taib Heakal, A.M. Fekry, M.Z. Fatayerji, *Electrochim. Acta*, 54 (2009): p. 1545.

31. L. Wang, T. Shinohara, B-P. Zhang, *J. Alloys and Compounds*, 496 (2010): p. 500.
32. G. Wu, Y. Fan, A. Atrens, C. Zhai, W. Ding, *J. Appl. Electrochem*, 38 (2008): p. 251.
33. F. El-Taib Heakal, A.M. Fekry, M. Abd El-Barr Jibril, *Corros. Sci.*, 53 (2011): p. 1174.
34. G. Williams, N. Birbilis, H.N. McMurray, *Electrochemistry Communications*, 36 (2013): p. 1.
35. G. Williams, K. Gusieva, N. Birbilis, *Corrosion*, 68 (2012): p. 489.
36. D.R. Lide, Editor, *CRC Handbook of Chemistry and Physics*, 78th Edition, p 4-68, CRC Press Inc., Boca Raton, USA (1997).
37. J.A. Boyer, Report-248, American Magnesium Corporation, Niagara Falls, NY, USA, 1927.
38. R.E. McNulty, J.D. Hanawalt, *Transactions of the Electrochemical Society*, 81 (1942): p. 423.
39. I. Lambert, H.L. Clever (Eds.), *IUPAC solubility data series*, Vol 52, Alkaline earth hydroxides in water and aqueous solutions, p. 104, Pergamon Press, Oxford UK (1992).
40. R. Tunold, H. Holtan, M-B. Hägg Berge, A. Lasson, R. Steen-Hansen, *Corros. Sci.*, 17 (1977): p. 353.
41. J. H. Nordlien, S. One, N. Masuko, K. Nisancioglu, *J. Electrochem. Soc.*, 142 (1995): p. 3320.
42. H.B. Yao, Y. Li, A.T.S. Wee, *Appl Surf. Sci.*, 158 (2000): p. 112.
43. M. Santamaria F. Di Quarto, S. Zanna, P. Marcus, *Electrochim. Acta* 53 (2007): p. 1314
44. M. Taheri, R.C. Phillips, J.R. Kish, G.A. Botton, *Corros Sci*, 59 (2012): p. 222.
45. G. Lorang, M. Da Cunha Belo, A. M. P. Simoes, M. G. S. Ferreira, *J. Electrochem. Soc.*, 141 (1994): p. 3347.
46. S. Y. Yu, W. E. O'Grady, D. E. Ramaker, P. M. Natishan, *J. Electrochem. Soc*, 147 (2000): p. 2952.

Figure 1

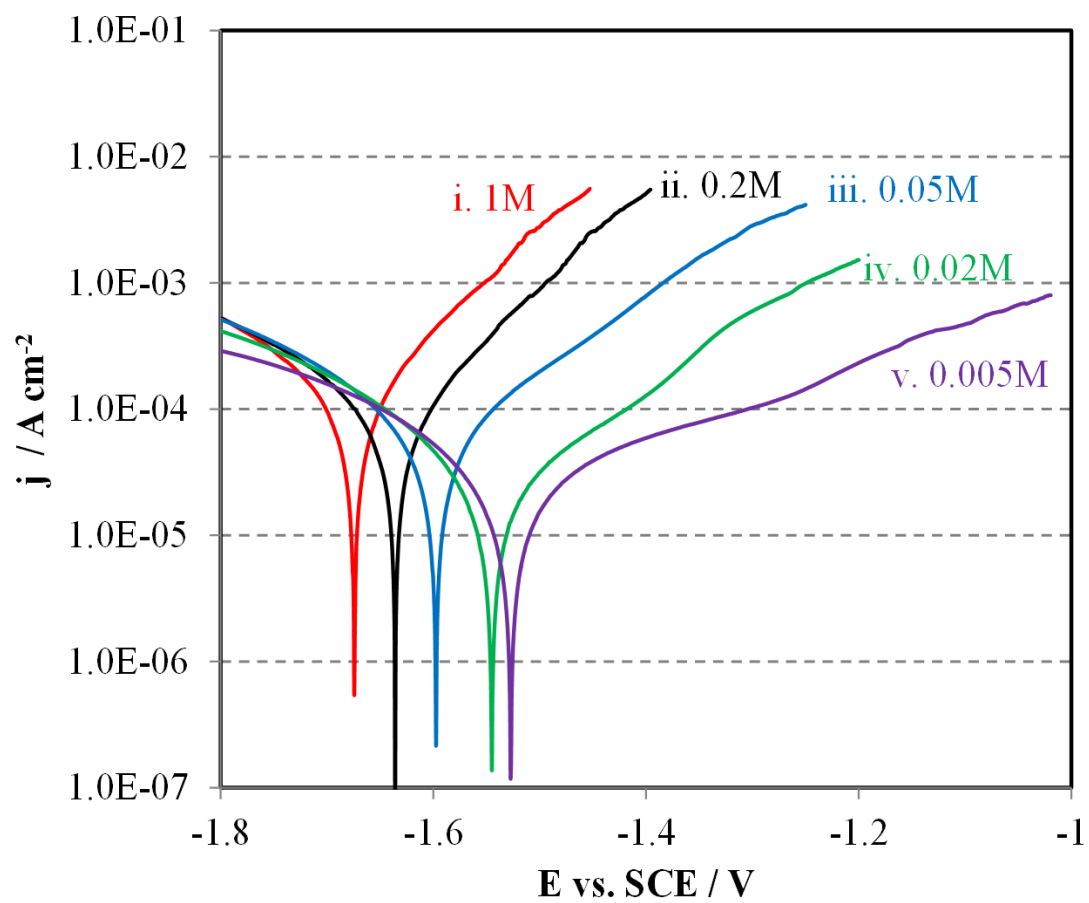


Figure 2

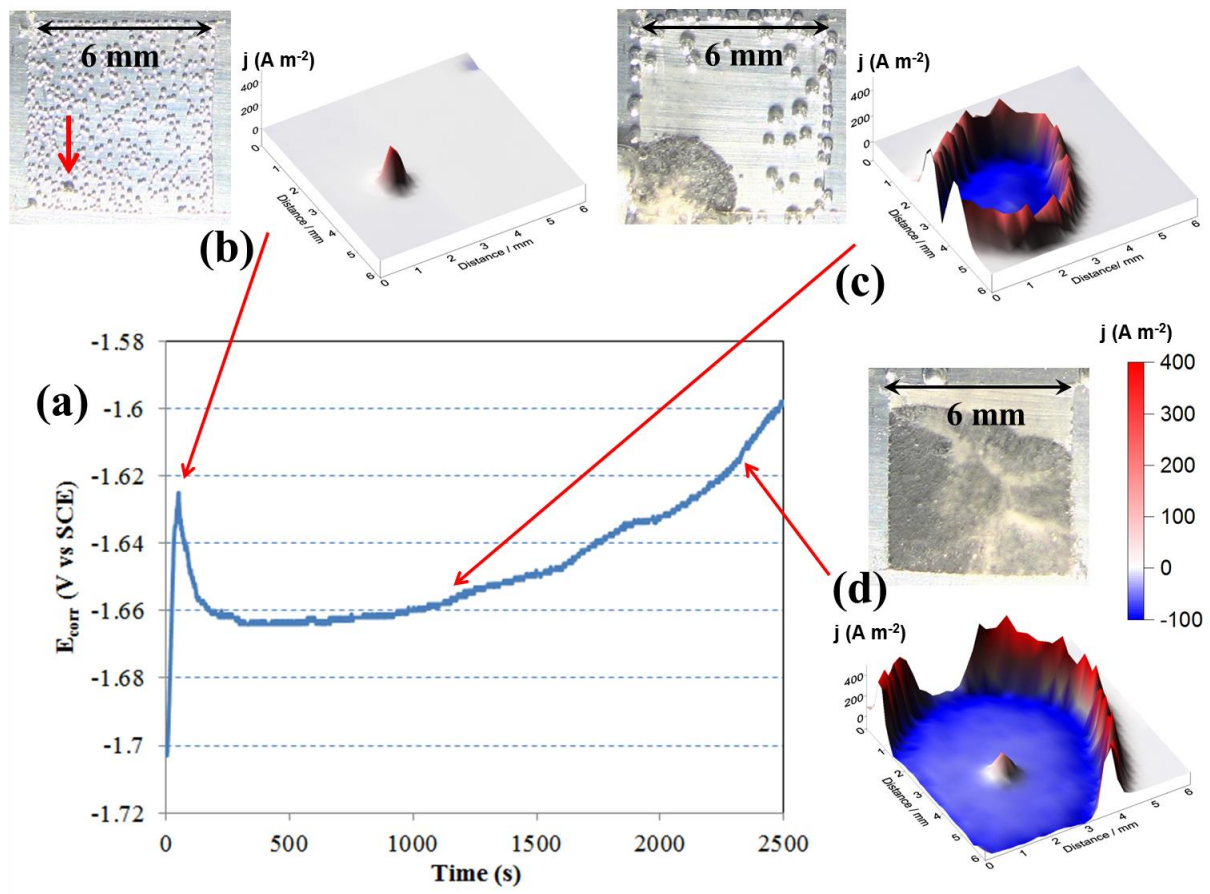


Figure 3

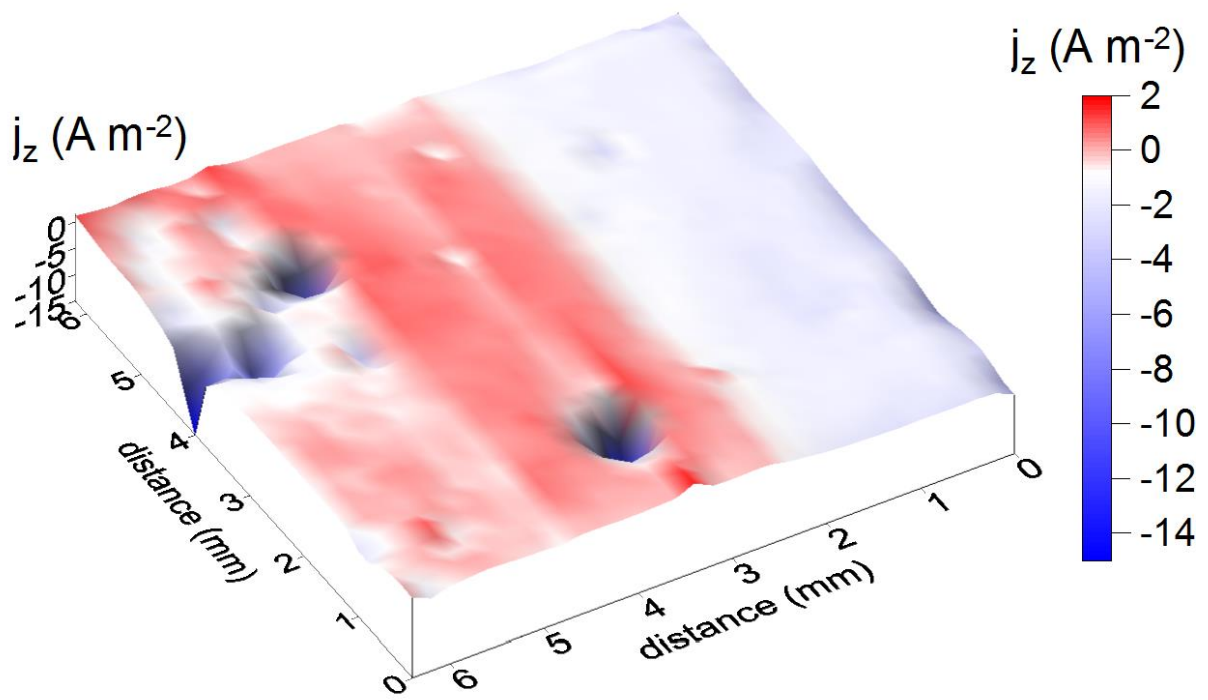


Figure 4

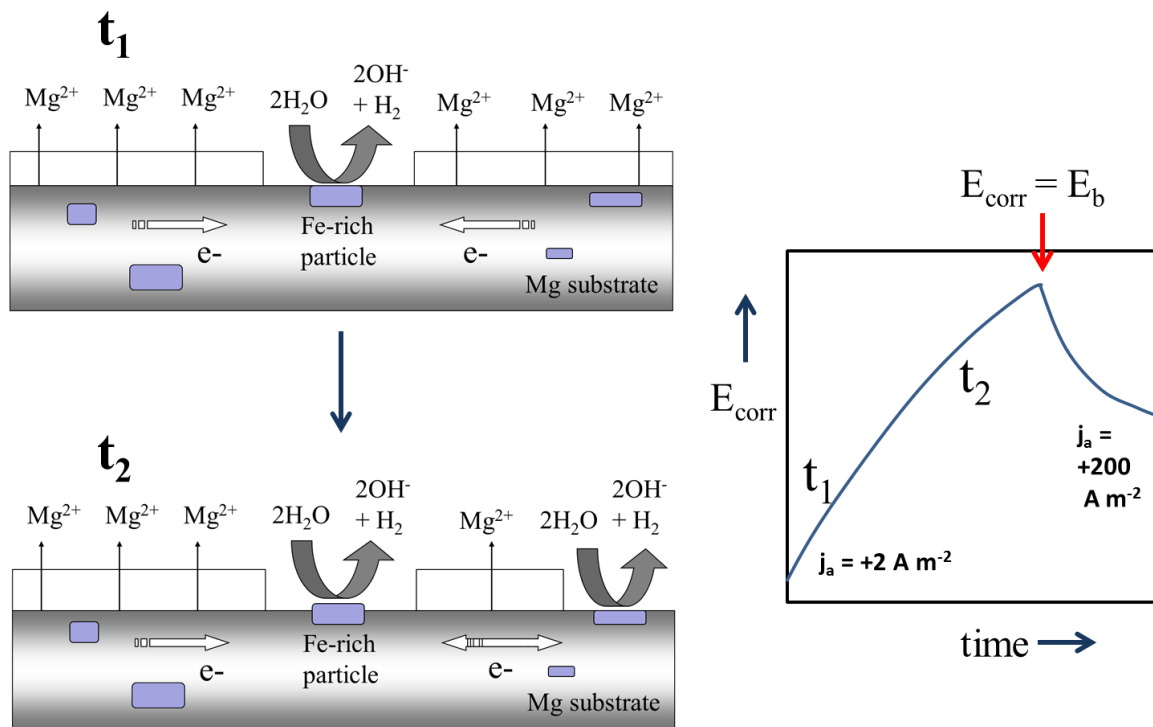


Figure 5

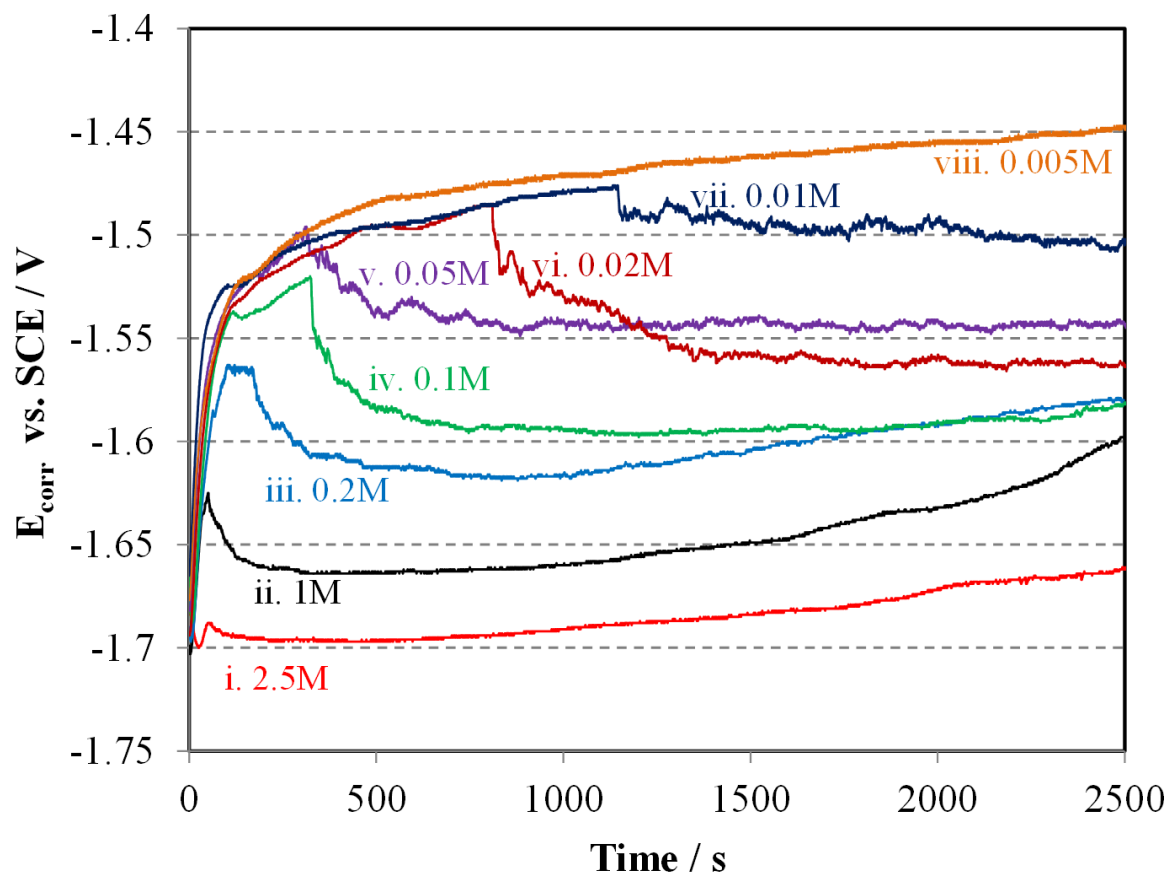


Figure 6

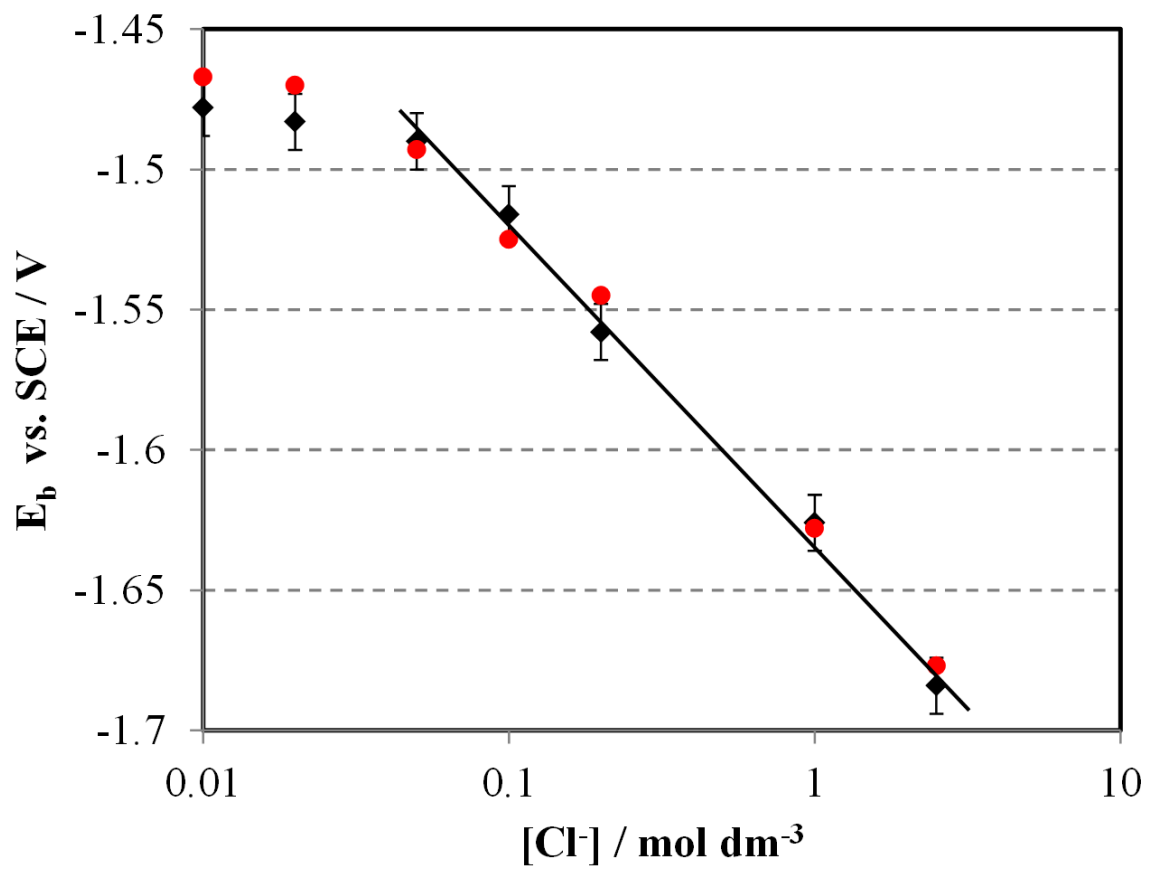


Figure 7a

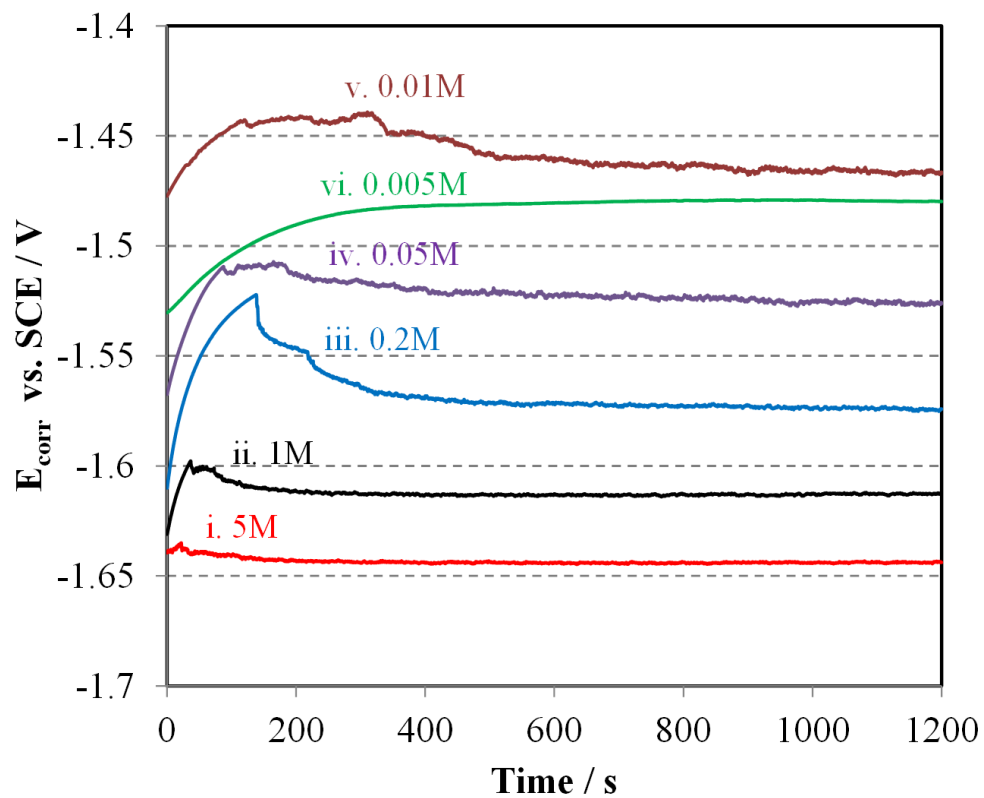


Figure 7b

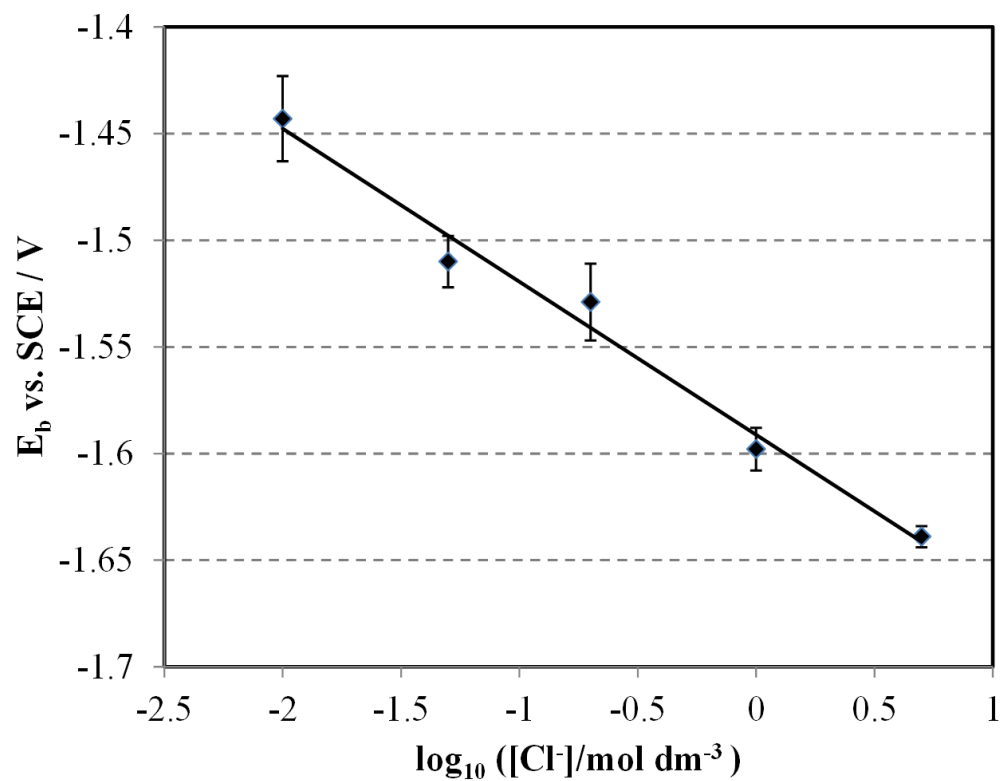


Figure 8a

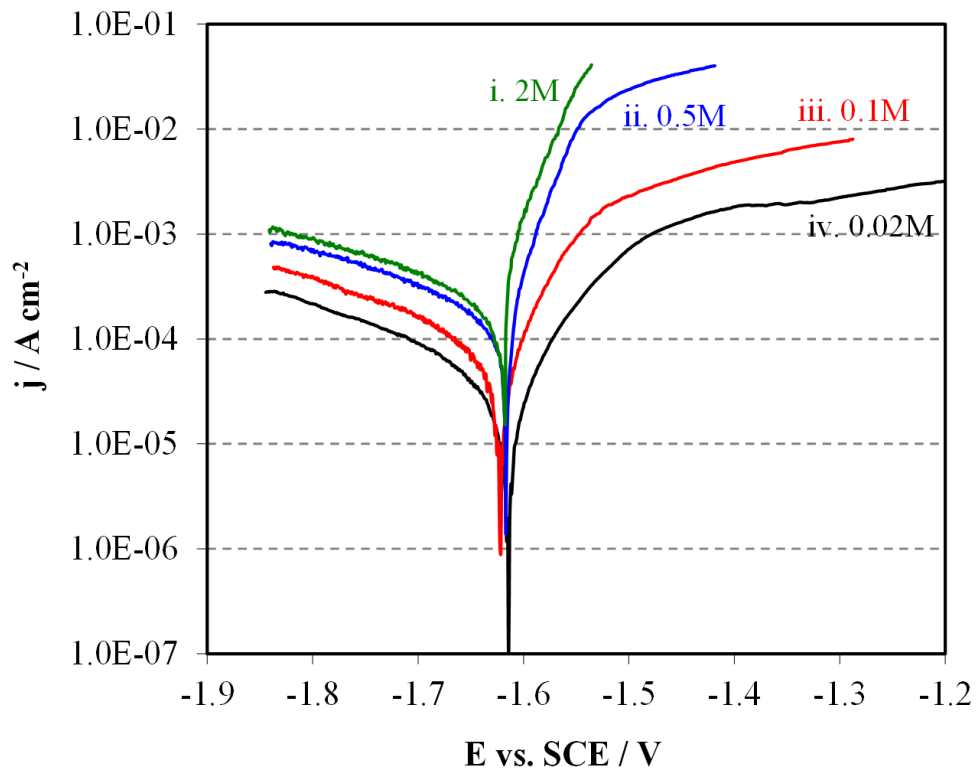


Figure 8b

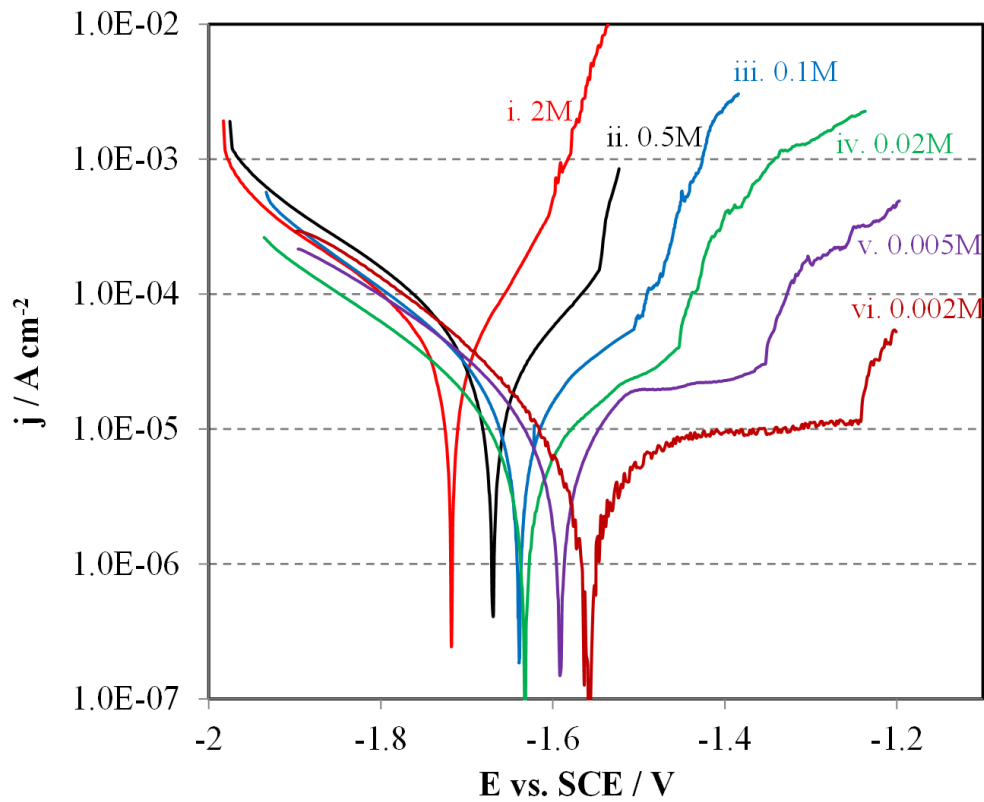


Figure 9

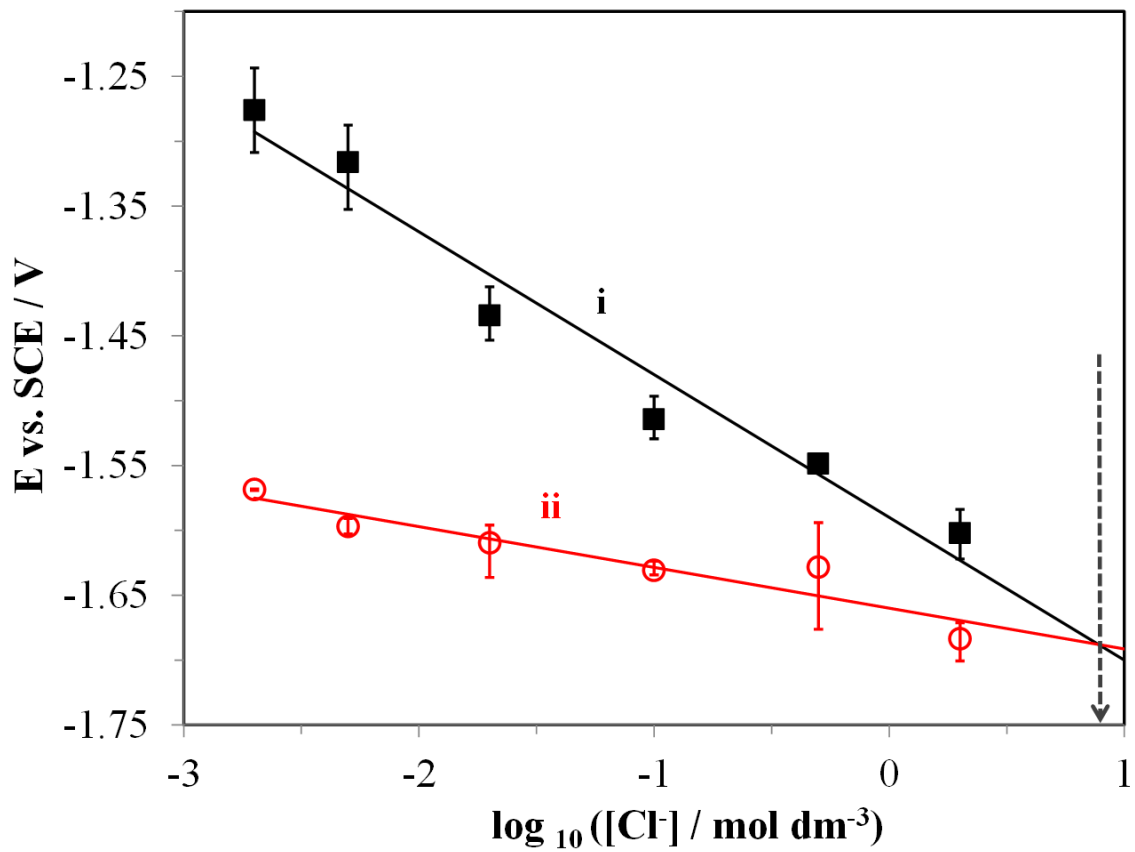


Figure 10

